Laurent, B., Deka, B., Hamida, Z. and Goulet, J-A. (Preprint 2023). *Analytical Inference for the Inspectors Uncertainty Using Network-Scale Visual Inspections.*

Analytical Inference for the Inspectors Uncertainty Using Network-Scale Visual Inspections.

Blanche Laurent*, Bhargob Deka, Zachary Hamida and James-A. Goulet
Department of Civil, Geologic and Mining Engineering
Polytechnique Montreal, CANADA

April 26, 2023

Abstract

Visual inspection is a common approach for collecting data over time on transportation infrastructure. However, the evaluation method in visual inspections mainly depends on a subjective metric, as well as the experience of the individual performing the task. State-space models (SSM) have enable quantifying the uncertainty associated with the inspectors while modelling the degradation of bridges based on visual inspection data. The main limitation in the existing SSM-model is the assumption that each inspector is unbiased, due to the high number of inspectors which makes the problem computationally demanding for optimization approaches, and prohibitive for sampling-based Bayesian estimation methods. The contribution of this paper is to enable the estimation of the inspector bias, and to formulate a new analytical framework that allows the estimation of the inspectors' biases and variances using Bayesian updating. The performance of the analytical framework is verified using synthetic data, where the true values are known, and validated using data from the network of bridges in Quebec province, Canada. The analyses have shown that the analytical framework has enabled reducing the computational time required for estimating the inspectors' uncertainty, and is adequate for the estimation of the inspectors' uncertainty, while maintaining a comparable performance to the gradient-based framework.

1 Introduction

Effective management and decision making on transportation infrastructure requires accurate measures for the health state of bridges over time [5, 20, 10]. For that purpose, structural health monitoring (SHM) is implemented to allow tracking the performance of bridges, by collecting and analyzing temporal data [1, 3]. Collecting data about the health state of bridges can be done by relying on different approaches, nonetheless, visual inspections are

*Corresponding author: blanche.laurent@polymtl.ca

considered as the default option [2, 29, 15, 11].

Visual inspections consist in on-site evaluations performed by inspectors who prospect for evidence of defects in the structural elements and assess the severity of their degradation condition [24]. The main advantage of visual inspections over other techniques is the capacity to provide a general evaluation for the structural condition that is not limited to a specific type of damage [22]. However, visual inspections have inherent limitations where the inspectors rely on subjective metrics in order to grade the health state of a structural element [15, 29]. Moreover, the difference in the experience of the inspector performing the inspection task leads to variability in visual inspection data, where some inspectors could have a tendency to overestimate the actual degradation state, while others to underestimate it [23, 25]. In addition, the frequency of inspections for a bridge is defined within a range from two to four years depending on structure's age among other factors, meaning that few inspection data is available over time [24, 17, 9, 21].

There are different types of degradation models that aim at improving the interpretability of visual inspection data and predict the condition of infrastructure over time [30, 4, 19, 6, 8, 28]. Out of the existing models, state-space models (SSM) have been effectively applied to model the degradation behaviour while partially taking into account the inspectors' uncertainty [14, 12]. The existing SSM framework neglects the bias associated with each inspector, which could affect the performance of the model given the limited inspections available per structural element. In addition, the SSM framework relies on a gradient-based approach for estimating the entire set of model parameters including the inspectors' uncertainty, which is computationally demanding.

The aim of this work is to improve the overall predictive capacity of the SSM-based degradation model by estimating the inspectors' relative biases, where *relative* indicates that the bias of one inspector is estimated in comparison with other inspectors, while assuming that on average all inspectors are unbiased. Furthermore, an analytical framework is proposed as a computationally efficient alternative to the gradient-based framework for estimating the inspectors' uncertainty. The proposed approach is based on approximate Gaussian variance inference (AGVI), which is an approximate analytical inference method [7]. The choice of AGVI over other Bayesian methods is mainly attributed to the fact that other Bayesian methods rely on either variational or sampling techniques, which can be computationally demanding in this context. This is because the number of variance parameters in the deterioration model is equivalent to the number of inspectors performing inspections on the entire network of bridges [12].

The overall performance of the modified degradation model is examined using a synthetic dataset and a real database from the Quebec province, Canada. The results and analyses have shown that including the inspectors' relative bias improves the performance of the degradation model. Moreover, the analytical framework provides a comparable performance with the gradient-based framework while significantly reducing the computational cost of estimating the inspectors' uncertainty.

1.1 Nomenclature

The SHM database encompass information about the visual inspections and interventions data from a network of $\mathtt{B}$ bridges represented by the set, $\mathcal{Q} = \{\mathcal{B}_1, \mathcal{B}_2, ..., \mathcal{B}_{\mathtt{B}}\}$, where each bridge $\mathcal{B}_j$ is composed of structural categories $\mathcal{B}_j = \{\mathcal{S}_1^j, \mathcal{S}_2^j, ..., \mathcal{S}_{\mathtt{S}_j}^j\}$, and each category is composed of structural elements $\mathcal{S}_s^j = \{e_1^j, e_2^j, ..., e_{\mathtt{E}_j}^j\}$. The structural attributes associated with each bridge $\mathcal{B}_j$ are represented by the set $\mathcal{Z} = \{z_1^j, z_2^j, ..., z_{\mathtt{Q}}^j\}$. Moreover, visual inspections provide data about the deterioration state of the elements in each bridge. Each inspection is performed at a year t, for an element e_p^j, by an inspector $I_i \in \mathcal{I} = \{I_1, I_2, \ldots, I_{\mathtt{I}}\}$. The inspector evaluates the condition $\tilde{y}$ of the elements on a scale from l to u, where l represents the worst condition possible of the element, while u represents the best condition possible.

2 Degradation Analyses using State-Space Models (SSM)

The SSM framework is employed to describe the deterioration process using the visual inspections data from each structural element e_p^j. The prediction and update steps in the SSM framework are performed using a *transition model* and an *observation model* [12]. Knowing the deterioration state at time $t-1$, the transition model predicts the deterioration state at time t,

$$\overbrace{\boldsymbol{x}_{t,p}^j = \boldsymbol{A}^{ki}\boldsymbol{x}_{t-1,p}^j + \boldsymbol{w}_t}^{\text{transition model}},\ \underbrace{\boldsymbol{w}_t : \boldsymbol{W} \sim \mathcal{N}(\boldsymbol{w}; \boldsymbol{0}, \boldsymbol{Q}^{ki})}_{\text{process error}}, \tag{1}$$

with $\boldsymbol{x}_{t,p}^j = [x_{t,p}^j, \dot{x}_{t,p}^j, \ddot{x}_{t,p}^j]^\intercal$ representing the hidden state vector containing the components, $x_{t,p}^j$ which represents the deterioration condition, $\dot{x}_{t,p}^j$ is the deterioration speed, and $\ddot{x}_{t,p}^j$ is the acceleration [12]. The matrix $\boldsymbol{A}^{ki}$ represents the kinematic model transition matrix, $\boldsymbol{w}_t$ is the normally distributed process error, and $\boldsymbol{Q}^{ki}$ is the covariance matrix of the process error; The aforementioned matrices are detailed in Appendix A. The hidden states estimates are updated by the inspection data $y_{t,p}^j$ using the observation model,

$$\overbrace{y_{t,p}^j = \boldsymbol{C}^{ki}\boldsymbol{x}_{t,p}^j + v_t}^{\text{observation model}},\ \underbrace{v_t : V \sim \mathcal{N}(v; 0, \sigma_V^2(I_i))}_{\text{observation error}}, \tag{2}$$

where $\boldsymbol{C}^{ki} = [1, 0, 0]$ is the observation vector, and v_t the observation error associated with the i-th inspector who has performed the inspection of the element e_p^j at time t [12]. Performing the hidden state estimation is done using the Kalman filter (KF) [18] and the RTS Kalman smoother [26], which are further detailed in Appendix A. The SSM deterioration model is extended to integrate the information about structural attributes

in the deterioration analyses by using Kernel Regression (KR) [13]. The KR role in the SSM-KR is to take advantage of the structural similarities (e.g., location, age, ..., etc.) across bridges in order to provide an estimate for the initial deterioration speed. The estimation for the initial deterioration speed in each structural element is done using,

$$\dot{x}^j_{0,p} = (\boldsymbol{a}^j_p)^\intercal \dot{\boldsymbol{x}}_z + w_0,\ W_0 \sim \mathcal{N}(w_0; 0, \sigma^2_{w_0}), \tag{3}$$

where w_0 is the process noise described by the variance $\sigma^2_{w_0}$, and $\boldsymbol{a}^j_p$ is a vector defined by,

$$\boldsymbol{a}^j_p = \frac{\boldsymbol{k}(z_j, \boldsymbol{Z}_{c(m)}, \boldsymbol{\ell})}{\Sigma^{\mathtt{M}^{\mathtt{Q}}}_{m=1}(\boldsymbol{k}(z_j, \boldsymbol{Z}_{c(m)}, \boldsymbol{\ell}))},\ m = 1, ..., \mathtt{M}^{\mathtt{Q}}, \tag{4}$$

with $\mathtt{Q}$ is the number of structural attributes, and $\boldsymbol{Z}_{c(m)} = [\boldsymbol{z}^1_c, \ldots, \boldsymbol{z}^{\mathtt{Q}}_c]$ is a $\mathtt{Q}-$dimensional grid discretized by $\mathtt{M}$ uniformly-spaced reference points [13]. The function $\boldsymbol{k}$ is a multivariate kernel function $\boldsymbol{k} : \mathbb{R}^{\mathtt{Q}} \to \mathbb{R}$ defined by,

$$\boldsymbol{k}(z_j, \boldsymbol{Z}_{c(m)}, \boldsymbol{l}) = k\left(\frac{z^1_j - \boldsymbol{z}^1_{c(m)}}{\ell_1}\right) \cdot ... \cdot k\left(\frac{z^{\mathtt{Q}}_j - \boldsymbol{z}^{\mathtt{Q}}_{c(m)}}{\ell_{\mathtt{Q}}}\right),\ m = 1, ..., \mathtt{M}^{\mathtt{Q}}, \tag{5}$$

where $k(.)$ is the univariate kernel function and $\boldsymbol{\ell} = [\ell_1 ... \ell_{\mathtt{Q}}]$ are the kernel length parameter for each covariate [13]. Determining the kernel length parameters along with other model parameters is done by using the *Maximum Likelihood Estimate* (MLE) approach Hamida:2020ab, which is further detailed in the next section. In order to ensure the monotonicity throughout the deterioration modelling process, the deterioration speed represented by $\dot{x}^j_{p,t} : \dot{X} \sim \mathcal{N}(\dot{\mu}^j_{p,t}, (\sigma^{\dot{x}})^2)$, is maintained within the negative domain according to the constraint, $\dot{\mu} + 2\sigma^{\dot{x}} \leq 0$. If the aforementioned constraint is violated at any time t, the PDF truncation method is applied to revise the hidden state estimate [27, 12]. Furthermore, the deterioration condition estimate $x^j_{t,p}$ is ensured to be within the feasible condition bounds $[l, u]$, by performing space transformation using the transformation function $o(\cdot)$ [12]. The transformation function $o(\cdot)$ enables mapping each point in the original bounded space $[l, u]$ to a point in the unbounded space such that, $o : [l, u] \to \mathbb{R}$. Further details about the transformation functions $o(\cdot)$ and its inverse $o^{-1}(\cdot)$ are provided in Appendix B. Figure 1 shows all the steps for modelling the deterioration of element e^j_p, starting from the element's inspection data $\tilde{\boldsymbol{y}}^j_{t,p}$, to the bounded degradation state estimate $\tilde{\boldsymbol{x}}^j_{t,p}$. From Figure 1, each element e^j_p has a set of inspections $\tilde{\boldsymbol{y}}^j_{t,p}$ and structural attributes $\boldsymbol{z}^j_p$. The structural attributes $\boldsymbol{z}^j_p$ can provide a prior estimate for the deterioration speed $\dot{\tilde{x}}^j_{0,p}$ by using KR as described in Equation 3. The transformation function $o(\cdot)$ is employed to perform the transformation on the inspection data $\tilde{\boldsymbol{y}}^j_{t,p}$ from the bounded space to the unbounded space, and obtain $\boldsymbol{y}^j_{t,p}$. Thereafter, the inspection data $\boldsymbol{y}^j_{t,p}$ and the prior estimate for the degradation state are provided to the SSM model to infer and predict the degradation state $\boldsymbol{x}^j_{t,p}$ over time. The degradation state $\boldsymbol{x}^j_{t,p}$ is back-transformed to the original bounded space by relying on the inverse transformation function $o^{-1}(\cdot)$. The set of parameters involved in the SSM-KR degradation model are described in the next section.

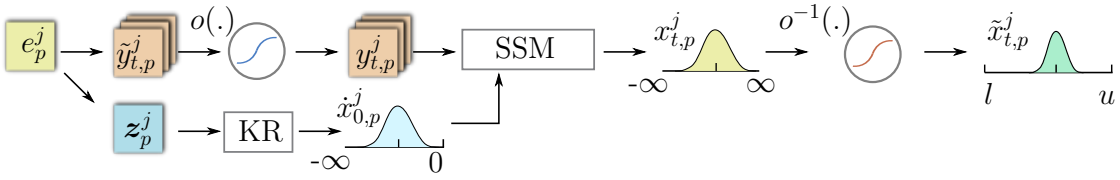

Figure 1: Flowchart for modelling the deterioration of element e_p^j, starting from the inspection data $\tilde{\boldsymbol{y}}_{t,p}^j$ and structural attributes $\boldsymbol{z}_p^j$. The inspection data are transformed using the step function $o(\cdot)$ to the unbounded space so that it is possible to model the deterioration behaviour using the SSM model. The SSM model also relies on the initial estimate of the deterioration speed $\tilde{\dot{x}}_{t,p}^j$ provided by the KR model. The end result of the framework is the bounded deterioration state estimate $\tilde{\boldsymbol{x}}_{t,p}^j$ which is obtained using the transformation function $o^{-1}(.)$.

2.1 Degradation Model Parameters and the Inspector Relative Bias

The full set of parameters to be estimated in the SSM-KR deterioration model [13] are,

$$\boldsymbol{\theta} = \{\sigma_V(I_{1:\mathtt{I}}), \sigma_W, n, \sigma_0, \ddot{\sigma}_0, p_1, p_2, \sigma_{w0}, \boldsymbol{\ell}\}\,, \tag{6}$$

where $\sigma_V(I_{1:\mathtt{I}})$ is the standard deviation of each inspector $I_i \in \mathcal{I}$, σ_W is the process error standard deviation, σ_0 and $\ddot{\sigma}_0$ are the standard deviations for the initial condition and initial acceleration respectively and p_1, p_2 are parameters associated with standard deviation of the initial deterioration speed [13]. The parameters σ_{w0} and $\boldsymbol{\ell}$ are related to the KR framework as described in the previous section [12, 13].
From the set of model parameters $\boldsymbol{\theta}$ and Equation 2, it can be noticed that the inspectors biases are omitted by assuming a zero-mean observation error for each inspector $I_i \in \mathcal{I}$. It is possible to bypass this simplification by estimating the relative bias for each inspector, where the word "relative" implies that while each inspector could have the tendency to overestimate or underestimate the true condition, the expected value for the biases from all inspectors is zero, $\mathbb{E}[\boldsymbol{\mu}_{b(i:\mathtt{I})}] = 0$. In this context, the observation error for any inspectors $I_i \in \mathcal{I}$ is defined by $v_t : V \sim \mathcal{N}(v; \mu_V(I_i), \sigma_V^2(I_i))$.
The relative bias for each inspector can be estimated using the same *Maximum Likelihood Estimate* (MLE) approach implemented originally in estimating the SSM-KR model parameters [13]. The log-likelihood in this context is defined as,

$$\mathcal{L}(\boldsymbol{\theta}) = \sum_{j=1}^{\mathtt{B}} \sum_{p=1}^{\mathtt{E}_j} \sum_{t=1}^{\mathtt{T}_p} \ln f(y_{t,p}^j | y_{1:t-1,p}^j, \boldsymbol{\theta}), \tag{7}$$

where $\mathtt{B}$ is the total number of bridges, $\mathtt{E}_j$ is the total number of structural element of the j-th bridge, and $\mathtt{T}_p$ is the total number of observation for the p-th element [12]. The full

formulation for optimizing the models parameters in $\boldsymbol{\theta}$ is,

$$\begin{aligned} \boldsymbol{\theta}^* &= \underset{\boldsymbol{\theta}}{\text{argmax}}\ \mathcal{L}(\boldsymbol{\theta}), \\ \text{subject to}: \ & \sigma_V^2(I_i) > 0, \forall I_i \in \mathcal{I}, \\ & -u < \mu_V(I_i) < u, \forall I_i \in \mathcal{I}, \\ & \sigma_W, n, \sigma_0, \ddot{\sigma}_0, p_1, p_2, \sigma_{w0}, \boldsymbol{\ell} > 0, \\ & n \in [1,2,3,4,5]. \end{aligned} \tag{8}$$

Solving the above mentioned problem is possible using an iterative gradient-based optimization method such as Newton-Raphson (NR) [16, 12]. Nonetheless, the main limitation of such an approach is the computational cost, especially as the number of inspectors increases. Moreover, as inspections are performed every year, the parameters need to be updated with the new data. In order to resolve these limitations, an analytical inference framework is proposed in this paper to enable the estimation of the inspectors' standard deviations as well as biases.

2.2 Analytical Inference for the Inspectors Uncertainty

The aim of the analytical inference framework is to provide a computationally-efficient alternative to the NR approach for estimating the inspectors' uncertainty. The basis of this framework relies on the analytical Gaussian variance inference (AGVI) approach [7], for estimating the variance parameters $\sigma_V^2(I_i)$, as well as a recursive framework for estimating the biases $\mu_V(I_i)$. The estimation of $\mu_V(I_i)$ and $\sigma_V^2(I_i)$ in this framework requires defining two additional hidden states: $v_b(I_i)$ to estimate $\mu_V(I_i)$, and $v_s(I_i)$ to estimate $\sigma_V^2(I_i)$ for each inspector $I_i \in \mathcal{I}$, where,

$$\begin{aligned} v_{b(i)} : V_{b(i)} &\sim \mathcal{N}(v_{b(i)}; \mu_{b(i)}, \sigma_{b(i)}^2), \\ v_{s(i)} : V_{s(i)} &\sim \mathcal{N}(v_{s(i)}; 0, \sigma_{s(i)}^2). \end{aligned} \tag{9}$$

It should be noted that by implementing this framework alongside the relative bias estimation framework, it is required to add a correction to the variance estimate $\sigma_{s(i)}^2$ by adding the variance of the bias $\sigma_{b(i)}^2$, such that, $\sigma_V^2(I_i) = \sigma_{s(i)}^2 + \sigma_{b(i)}^2$. The inference of the aforementioned parameters is done alongside the inference of the degradation states within the SSM framework. This is achieved by updating the hidden states $V_{b(i)}$ and $V_{s(i)}$, associated with the inspector I_i, whom has performed the inspection at time t. Accordingly, the state vector $\boldsymbol{x}_{t,p}^j$ at time t is augmented to include the additional hidden states, such that $\boldsymbol{x}_{t,p}^j = [\boldsymbol{x}^{ki}; v_b(I_i); v_s(I_i)]^\intercal$, where $\boldsymbol{x}^{ki}$ are the hidden states associated with the kinematic model of the degradation. This adjustment results in modifying the transition matrix $\boldsymbol{A}$, and the process error covariance matrix $\boldsymbol{Q}$ so that,

$$\boldsymbol{A} = \begin{bmatrix} \boldsymbol{A}^{ki} & \boldsymbol{0}_{2\times 2} \\ \boldsymbol{0}_{2\times 2} & \boldsymbol{I}_{2\times 2} \end{bmatrix}, \quad \boldsymbol{Q} = \begin{bmatrix} \boldsymbol{Q}^{ki} & \boldsymbol{0}_{2\times 2} \\ \boldsymbol{0}_{2\times 2} & \boldsymbol{0}_{2\times 2} \end{bmatrix}, \tag{10}$$

where $\boldsymbol{I}$ represents the identity matrix. The observation matrix $\boldsymbol{C}$ is also modified to account for the changes in $\boldsymbol{x}_{t,p}^{j}$ as in, $\boldsymbol{C}_t = [\boldsymbol{C}^{ki}, 1, 1]$. The estimation for the hidden states $v_b(I_i)$ and $v_s(I_i)$ is done simultaneously using the frameworks described in the next sub-sections. It should be noted that the inspectors errors are considered to be independent, and the inspector performance over time is assumed to be stationary.

2.2.1 Estimating the Relative Bias for Each Inspector

In this framework, the estimation for the relative-bias $\mu_V(I_i)$ is done recursively by estimating the hidden states $\boldsymbol{v}_b(I_i)$ for all inspectors $I_i \in \mathcal{I}$, based on the inspection data from all structural elements e_p^j. The initialization for the hidden states $\boldsymbol{v}_b(I_i)$ is done based on a weakly-informative prior with an expected value for the initial bias, $\mu_{b(i)} = 0$, and an initial variance $\sigma^2_{b(i)} = 4$, for each inspector $I_i \in \mathcal{I}$. Following the initialization step, the analytical inference framework is applied, where the state $v_b(I_i)$ is updated based on the inspection data $\boldsymbol{y}_{t,p}^{j}$ on element e_p^j from inspector I_i. The updated state estimate of $v_b(I_i)$ is then employed as a prior in the analyses of structural element e_{p+1}^j, which enables updating the state $v_b(I_i)$, with another set of inspection data from the same inspector I_i. The sequential updates are carried out simultaneously for all inspectors $I_i \in \mathcal{I}$, down to the last structural element with inspection data. It should be noted that during the estimation for the relative bias $V_{b(i)}$, the expected value for the initial condition $\mu_{0,p}^{j}$ of each element e_p^j is considered as a ratio of the maximum observation as, $\mu_{0,p}^{j} = \left(1 - \frac{|\mathbb{E}[\boldsymbol{\mu}_{b(1:\mathrm{I})}]|}{u-l}\right) \times \max(\boldsymbol{y}_{t,p}^{j})$. The aforementioned initialization mitigates the likelihood of activating the deterioration speed constraints described in Section 2, and is found empirically to yield overall good estimation results.

2.2.2 Estimating the Variance for Each Inspector

Estimating the variance parameters $\sigma_V^2(I_i)$ is done using the AGVI approach [7], and by learning the hidden state $v_s(I_i)$ for each inspector $I_i \in \mathcal{I}$. The inference for $v_s(I_i)$ is done by relying on the theoretical definition of the variance such that, $\mathrm{var}[V_{s(i)}] = \mathbb{E}[V_{s(i)}^2] - \mathbb{E}[V_{s(i)}]^2$. The AGVI approach is derived based on the assumption that $\mathbb{E}[V_{s(i)}] = 0$; therefore, the variance for each inspector can be represented by, $\mathrm{var}[V_{s(i)}] = \mathbb{E}[V_{s(i)}^2]$. As a result, the hidden state $v_s(I_i)$ is infered by estimating $\mathbb{E}[V_{s(i)}^2]$. The expected value $\mathbb{E}[V_{s(i)}^2]$ can be modelled as a random variable $V_{\bar{\nu}(i)} \sim \mathcal{N}(\mu_{\bar{\nu}(i)}, \sigma^2_{\bar{\nu}(i)})$, where it has been demonstrated that $\sigma^2_{s(i)} = \mu_{\bar{\nu}(i)}$[7]. Moreover, according to the Gaussian multiplication approximation (GMA) [7], the variable $V_{s(i)}^2$ can be approximated by a Normal variable described by

$V_{\nu(i)} \sim \mathcal{N}(\mu_{\nu(i)}, \sigma^2_{\nu(i)})$, where at any time t,

$$\begin{aligned} \mu_{\nu(i),t|t} &= \mu^2_{s(i),t|t} + \sigma^2_{s(i),t|t}, \\ \sigma^2_{\nu(i),t|t} &= 2\sigma^4_{s(i),t|t} + 4\left(\mu^2_{s(i),t|t} \times \sigma^2_{s(i),t|t}\right). \end{aligned} \tag{11}$$

It should be noted that for clarity, the notation ν is used to refer to the hyper-parameters describing the square of the inspectors uncertainty $V^2_{s(i)}$, while $\bar{\nu}$ refers to the hyper-parameters describing the expected value of the square of the inspector uncertainty $\mathbb{E}[V^2_{s(i)}]$.

At time $t = 0$, the variance $\sigma^2_{s(i)}$, is assumed to be equal to the initial variance estimate for each inspector σ^2_V, where $\sigma^2_{s(i)} = \mu_{\bar{\nu}(i)} = \sigma^2_V$. On the other hand, the variance $\sigma^2_{\bar{\nu}(i)}$ is considered as, $\sigma^2_{\bar{\nu}(i)} = 12^2$, which represents weakly-informative prior value for $v_{\bar{\nu}}(I_i)$. The transitions of the hidden states $v_s(I_i)$ are handled directly by the transition model described in Equation 1, while using the modified transition matrix $\boldsymbol{A}$ [7]. However, the transition of the variable $v_\nu(I_i)$ from time $t-1$ to t is expressed by,

$$\begin{aligned} \mu_{\nu(i),t|t-1} &= \mu_{\bar{\nu}(i),t-1|t-1}, \\ \sigma^2_{\nu(i),t|t-1} &= 3\sigma^2_{\bar{\nu}(i),t-1|t-1} + 2\mu_{\bar{\nu}(i),t-1|t-1}. \end{aligned} \tag{12}$$

Following the transitions, the updates for the hidden states $v_s(I_i)$ are done based on the updates of the hidden state $v_{\bar{\nu}}(I_i)$ such that,

$$\begin{aligned} \mu_{\bar{\nu}(i),t|t} &= \mu_{\bar{\nu}(i),t|t-1} + K_\nu\left(\mu_{\nu(i),t|t} - \mu_{\nu(i),t|t-1}\right), \\ \sigma^2_{\bar{\nu}(i),t|t} &= \sigma^2_{\bar{\nu}(i),t|t-1} + K^2_\nu\left(\sigma^2_{\nu(i),t|t} - \sigma^2_{\nu(i),t|t-1}\right), \end{aligned} \tag{13}$$

where K_ν is defined as $K_\nu = \frac{\sigma^2_{\nu(i),t-1|t-1}}{\sigma^2_{\nu(i),t|t-1}}$ [7]. The above equations are computed for each inspector independently, and at each time step where an inspection data is available. The estimation of the hidden states $v_b(I_i)$ and $v_s(I_i)$ is done sequentially and over multiple epochs. The modified parameter estimation framework is detailed in the pseudo-code in Appendix D. Moreover, further details about the analytical framework are provided in the flowchart in Appendix C.

3 Visual Inspections Database

This section provides an overview for the network-scale visual inspection database, as well as the concepts employed in generating synthetic visual inspection dataset.

3.1 Visual Inspections - Real Case

The database includes reports of visual inspections and interventions on structural elements from the network of bridges $\mathcal{Q}$. In general, visual inspections are performed on-site and using standard techniques described in the *inspections manual* [24]. The inspector evaluates and records the deterioration condition of a structural element based on four levels of damage severity, which are: A: *Nothing to little*, B: *Medium*, C: *Important* and D: *Very Important* [24]. An example case for an inspection report is, $y_a = 60\%,\ y_b = 20\%,\ y_c = 15\%,\ y_d = 5\%$, which translates to 60% of the structural element area has no damage, 20% has medium damage, 15% has an important damage and 5% has a very important damage. Note that the sum of the ratios from each damage category must adhere to, $y_a + y_b + y_c + y_d = 100\%$, where, $0\% \leq y_a, y_b, y_c, y_d \leq 100\%$. Since the deterioration process is monotonic, it is possible to aggregate the damage categories into a single measure using,

$$\tilde{y} = \omega_1 y_a + \omega_2 y_b + \omega_3 y_c + \omega_4 y_d, \tag{14}$$

where $\omega_1 = 100$, $\omega_2 = 75$, $\omega_3 = 50$, $\omega_4 = 25$ representing the serviceability for each damage level, and $\tilde{y}$ is the aggregated observation [12]. Using the aforementioned aggregation approach, each inspection $\tilde{y}$ becomes a continuous numerical value with $\tilde{y} \in [25, 100]$, where $\tilde{y} = 100$ is equivalent to a perfect state ($y_a = 100\%, y_b = 0\%, y_c = 0\%, y_d = 0\%$), and $\tilde{y} = 25$ is equivalent the worst state ($y_a = 0\%, y_b = 0\%, y_c = 0\%, y_d = 100\%$).

3.2 Synthetic Visual Inspections

Verifying the proposed framework is possible by using synthetic data, where the true inspectors parameters as well as the true deterioration condition are available. The synthetic dataset resembles the real database quantitatively and qualitatively, where a set of predefined criterion are maintained [12]. The true deterioration state of $\mathtt{E} = 18000$ synthetic elements is generated over a lifespan of $\mathtt{T} = 60$ years, based on the transition model defined in Equation 1, and by using $\sigma_w = 5 \times 10^{-3}$. In this context, the deterioration condition is represented by a continuous numerical value where $\tilde{y} \in [25, 100]$. The inspection data are generated using the observation model in Equation 2 and based on $\mathtt{I} = 250$ synthetic inspectors, where each inspector $I_i \in \mathcal{I}$ has an observation error described by, $v^j_{t,p} : V \sim \mathcal{N}(v; \mu_V(I_i), \sigma_V(I_i))$. The bias $\mu_V(I_i)$ and standard deviation $\sigma_V(I_i)$ are generated for each inspector using a Uniform distribution where, $\sigma_V(I_i) \sim \mathcal{U}(1, 6)$, and $\mu_V(I_i) \sim \mathcal{U}(-4, 4)$. The total number of inspections per element range from 3 to 5 observations over time for the majority of elements, with few structural elements having 8-10 observations.

4 Case Studies

This section presents the case studies the are employed for verifying and validating the proposed approach for inferring the inspectors' uncertainty. These case studies are intended

to quantify the gain of performance obtained by including the inspector's biases into the degradation analyses, as well as comparing the predictive capacity of the SSM-based model while using the parameters estimated from the analytical or the gradient-based framework. In order to distinguish the sets of parameters estimated by each framework, the following notation are defined :

- The set of parameter using the gradient-based framework while considering unbiased inspectors, $\boldsymbol{\theta}^{G-} = \{\mu_v(I_{i:\mathtt{I}}) = 0, \sigma_v(I_{i:\mathtt{I}})\}$,
- The set of parameter using the gradient-based framework while considering biased inspectors, $\boldsymbol{\theta}^{G} = \{\mu_v(I_{i:\mathtt{I}}), \sigma_v(I_{i:\mathtt{I}})\}$,
- The set of parameter using analytical framework, $\boldsymbol{\theta}^{A} = \{\mu_{b(i:\mathtt{I})}, \mu_{\bar{\nu}(i:\mathtt{I})}\}$.

Finally the computational time required for estimating the inspectors' uncertainty parameters $\boldsymbol{\theta}^v$ is denoted as t_c.

4.1 Verification Analyses Using Synthetic Data

In this section, the synthetic database described in Section 3.2 is used to verify the capacity of the gradient-based framework to estimate the inspectors' biases as well as the effect of considering the bias on the predictive capacity of the degradation model. Therafter, the proposed analytical framework is employed to estimate the inspectors' uncertainty from the same database in order to compare its performance with the gradient-based framework.

4.1.1 Estimating the Synthetic Inspectors' Uncertainty Using the Gradient-Based Framework

Verification analyses are performed to study the capacity of the gradient-based framework to estimate the inspectors' biases, as well as the effects of including the biases on the predictive capacity of the SSM-KR model. Figure 2 shows the set of estimated parameters $\boldsymbol{\theta}^{G}$ and $\boldsymbol{\theta}^{G-}$, where the scatter plots show a comparison between the estimated parameters versus the true values of both, the inspectors' standard deviations and biases. From Figure 2a, in view of the concentration of the estimated biases and standard deviations along the diagonal, it is possible to conclude that the gradient-based framework is effective in estimating the model parameters associated with each inspector. This is validated by the accuracy measures reported in Figures 2a and 2b, where the coefficient of determination R^2 is near 90% and the root mean square error (RMSE) is close to zero. Moreover, it can be noticed from Figures 2b and 2c, that omitting the bias in the previous framework affects the quantification of the inspectors' uncertainty. This is because when the biases are neglected, the standard deviation increase to account for the additional variability resulting from biases.

The aforementioned sets of parameters are used separately in the SSM-based model in order

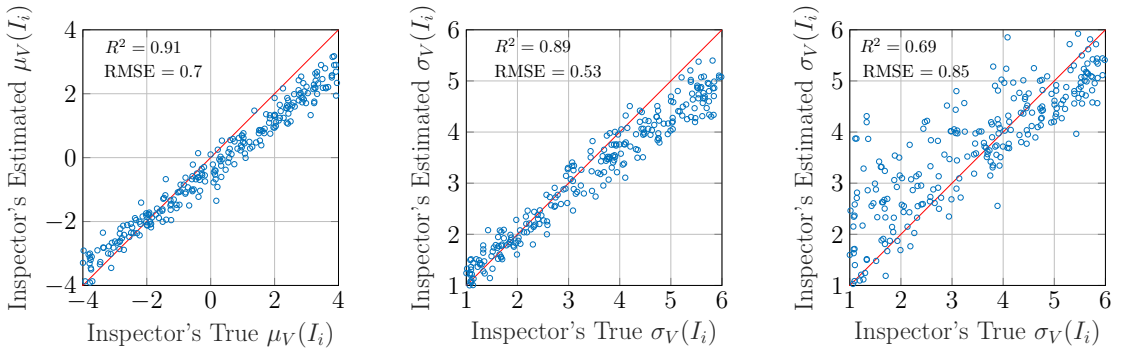

(a) Estimated biases from $\boldsymbol{\theta}^G$

(b) Estimated standard deviations from $\boldsymbol{\theta}^G$

(c) Estimated standard deviations from $\boldsymbol{\theta}^{G-}$

Figure 2: Results for the estimation of all inspectors' parameters using the gradient-based framework, the biases $\mu_V(I_i)$ (a), and the standard deviations $\sigma_V(I_i)$ (b) while considering the biased inspectors and $\sigma_V(I_i)$ (c) while considering unbiased inspectors , compared to their true value. Each figure is accompanied by accuracy measures, which include the coefficient of determination R^2 and the root mean square error (RMSE).

to evaluate the effect of including the bias in the degradation model. Figure 3 shows an example of the degradation analyses performed on the synthetic element e_1^{16}, where Figure 3a represents the analysis when neglecting the bias, and 3b shows the degradation condition, when including the bias. The cyan points correspond to the synthetic inspection data, and the blue asterisks represent the observations corrected with the bias estimated for each inspector. The black dashed line is the true degradation condition of the elements, while the red dashed line is the expected value of the condition from the model analyses, and the shaded areas represent the confidence interval for σ_{Model} and $2\sigma_{Model}$. In this example, the framework that considers biases is closer to the true state compared with the framework without biases, indicating that the inclusion of the bias in the degradation analyses has improved the predictive performance in this case.

In order to assess the network-scale performance of including the biases, Figure 4 compares the error in the predictions between the framework considering or neglecting the biases. The errors in the degradation condition estimates are computed following $\sum_{p=1}^{\mathtt{E}}(x_{t,p}^j - \mu_{t|T,p}^j)/\mathtt{E}$, and for the speed following $\sum_{p=1}^{\mathtt{E}}(\dot{x}_{t,p}^j - \dot{\mu}_{t|T,p}^j)/\mathtt{E}$. By comparing Figure 4a and 4b, the average forecast errors for both the condition and speed are smaller for the framework that accounts for the inspector bias, compared with the one with $\mu_V(I_i) = 0$. Therefore, we can conclude that the inclusion of the biases is improving the overall predictive capacity of the SSM-based degradation model.

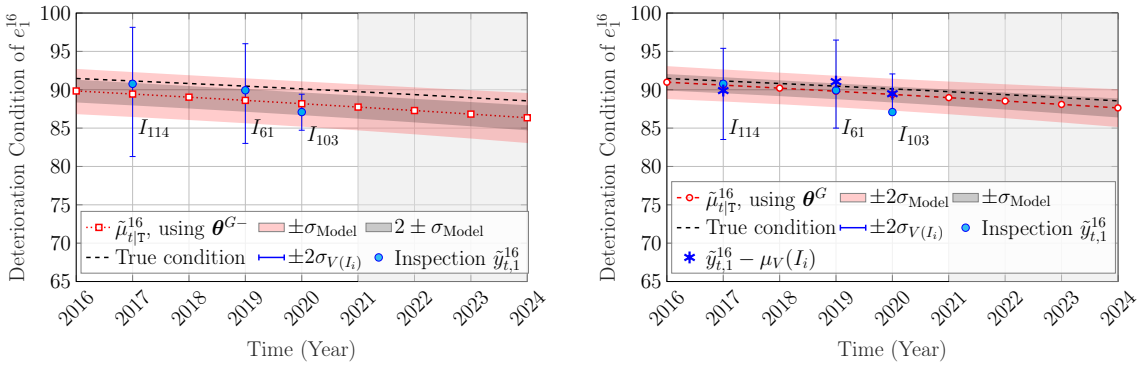

(a) Analyse perform using $\boldsymbol{\theta}^{G-}$ (b) Analyse perform using $\boldsymbol{\theta}^{G}$

Figure 3: Degradation condition analysis from synthetic inspection data $\tilde{y}^{16}_{t,1}$ of a synthetic structural element e_1^{16}, while neglecting the bias (a) and including the bias (b). The black dashed line represents the true condition, while the red one is the estimated condition. The shaded areas represent the confidence interval for σ_{Model} and $2\sigma_{Model}$.

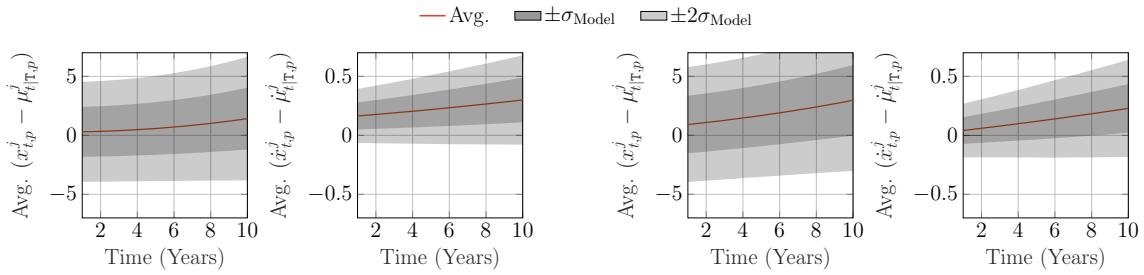

(a) Error while neglecting inspectors' bias (b) Error while considering inspectors' bias

Figure 4: Average error in forecast for the degradation condition and speed, over 10 years, for the gradient-based framework, while including the bias (a), and without biases (b), with the confidence interval for the estimation $\pm 2\sigma$.

4.1.2 Estimating the Synthetic Inspectors' Uncertainty Using the Analytical Framework

Verification analyses are performed in this section to study the capacity of the analytical framework to estimate the inspectors' uncertainty compared with the gradient-based framework. An example of application of the analytical inference framework for a single inspector I_{143} is shown in Figure 5. From this figure, the bias estimates from all the observations associated with the inspector I_{143} are shown, where the initial state, defined by $\mu_b = -1.17$ and $\sigma_b = 1.57$, is the result of the last epoch of the analytical inference framework. Similarly, Figure 5b shows the estimation process of the standard deviation $\sigma_V(I_{143})$. The analytical framework relies on more than one epoch, and the expected values for the hidden state v_b and the hyper-parameter $v_{\bar{\nu}}$ obtained at the end of one epoch serve as prior for the expected values μ_b and $\mu_{\bar{\nu}}$ for the next epoch. On the other end, the standard deviations for both hidden states are reinitialized using their prior $\sigma_b = 1$, and $\sigma_{\bar{\nu}} = 12$ to avoid early convergence. The true values for the bias and standard deviation, which are represented by red dashed lines, are within in the confidence interval of the estimated values, which confirms the quality of these estimates.

Figure 6 presents the expected values of the estimated hidden states for all inspectors compared with the true values of the inspectors' uncertainty. The alignment with the diagonal line in Figures 6a and 6b confirm the capacity of the analytical framework to estimate the inspectors' uncertainty. The coefficient of determination R^2 in this case is near 80% and the root mean square error (RMSE) is at 0.66 for the estimated standard deviations and 1.05 for the estimated biases. By comparing the results from Figures 6 and 2, it is possible to conclude that the estimation of the inspectors' parameters is more accurate when using the gradient-based framework; however, the results from the analytical framework is still consistent with the true parameters' value. Moreover, the hidden states associated with the inspectors' uncertainty are estimated using only 4 epochs compared with a total of 3000 epochs for the parameters using the gradient-based method (shown in Figure 2). This is mainly attributed to the fact that in a single epoch, the analytical inference enables updating the value of all the inspectors' hidden states at once. On the other hand, the gradient-based framework requires multiple epochs for updating the parameters associated with each inspector. Consequently, the computational time associated with estimating the inspectors' parameters is $t_c = 6$ minutes using the analytical framework compared with $t_c = 1140$ minutes using the gradient-based framework. The computational times are assessed based on a system equipped with CPU Intel Xeon CPU E5-2687W v4, 256GB memory and NVIDIA Tesla P40 GPU.

In order to evaluate the SSM-KR performance using the aforementioned parameters, Figure 7 presents the average forecast errors on the degradation condition and speed over the span of 10 years for the analytical framework. The black dashed line represents the error associated with the gradient-based framework presented in Figure 4b. From Figure 7a, it can be noted that the loss in the precision for the prediction of the condition and speed

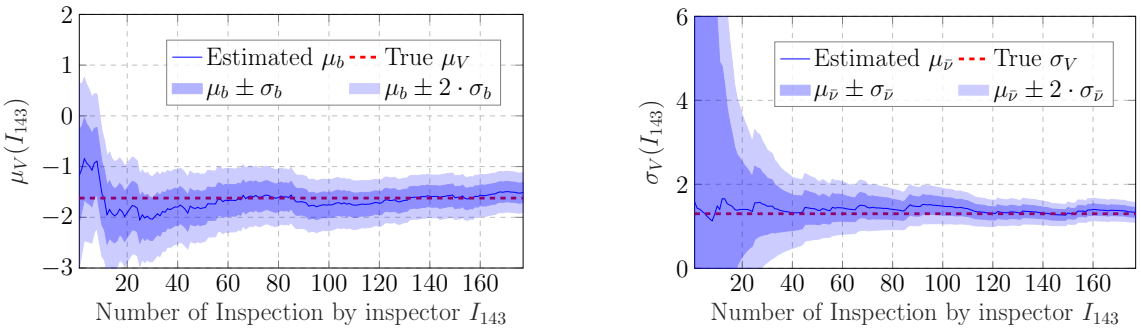

(a) Estimated bias

(b) Estimated standard deviation

Figure 5: Estimation process of the uncertainty parameters of inspector I_{143}, the bias $\mu_V(I_{143})$ in (a), and the standard deviation $\sigma_V(I_{143})$ in (b), using the analytical framework, with the parameters' true value represented by the dashed line, and the blue area representing the uncertainty associated with the estimation.

when replacing the gradient-based framework by the analytical one is not significant. The performance of the SSM-based model is not affected by loss in accuracy on the parameter estimation from the analytical framework. Consequently, it is possible to conclude that even though the performance of the gradient based framework is better, the analytical framework is acceptable for the estimation of the inspectors' uncertainty.

4.2 Validation Analyses Using Real Database

The real database in this study is composed of visual inspections from year 2007 up to 2019, corresponding to $\mathtt{E} = 51955$ *beam* elements from $\mathtt{B} = 5998$, bridges. The structural attributes $\boldsymbol{z}_j$ employed within this degradation analyses are: z_j^1 the elements material, z_j^2 the age of the structure, z_j^3 the bridge's location represented by the latitude and z_j^4 the structural element's condition. The selection of the aforementioned attributes is based on the kernel length $\boldsymbol{\ell}$, estimated using a MLE approach [13]. In order to perform the parameter estimation, the database is divided into three independent sets of bridges, 1) the training set containing $\mathtt{E_{tr}} = 42374$ elements from $\mathtt{B_{tr}} = 1915$ bridges, 2) validation set with $\mathtt{E_v} = 6388$ elements from $\mathtt{B_v} = 142$ bridges and a testing set with $\mathtt{E_t} = 3193$ structural elements from $\mathtt{B_t} = 76$ bridges.

4.2.1 Real Inspectors' Uncertainty Quantification Using the Gradient-Based Framework

Figure 8a and 8b show the histograms of the estimated inspectors' parameters $\boldsymbol{\theta}^G$, while Figure 8c shows the histogram of the estimated standard deviations based on $\boldsymbol{\theta}^{G-}$ for the framework considering unbiased inspectors. In Figure 8a, the average of the estimated

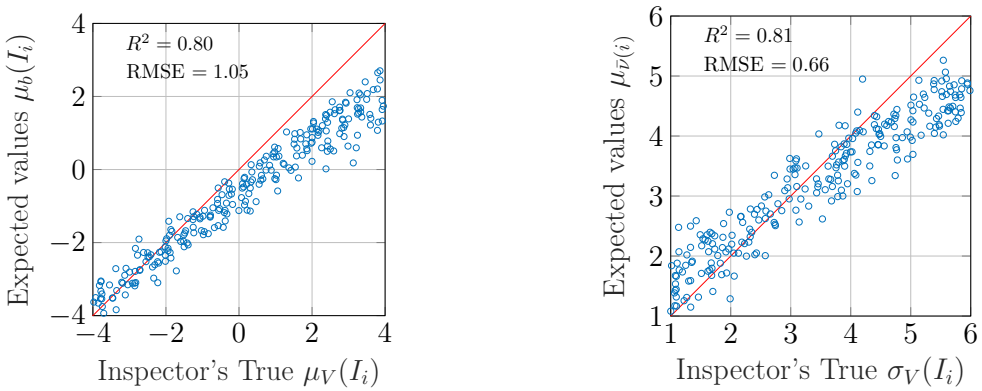

(a) Estimated biases

(b) Estimated standard deviations

Figure 6: Results for the estimation of all inspectors' hidden states, the biases $\mu_{b(i)}$ in (a), and the standard deviations $\mu_{\bar{\nu}(i)}$ in (b), compared to their true value using the analytical framework. Each figure is accompanied by accuracy measures, which include the coefficient of determination R^2 and the root mean square error (RMSE)

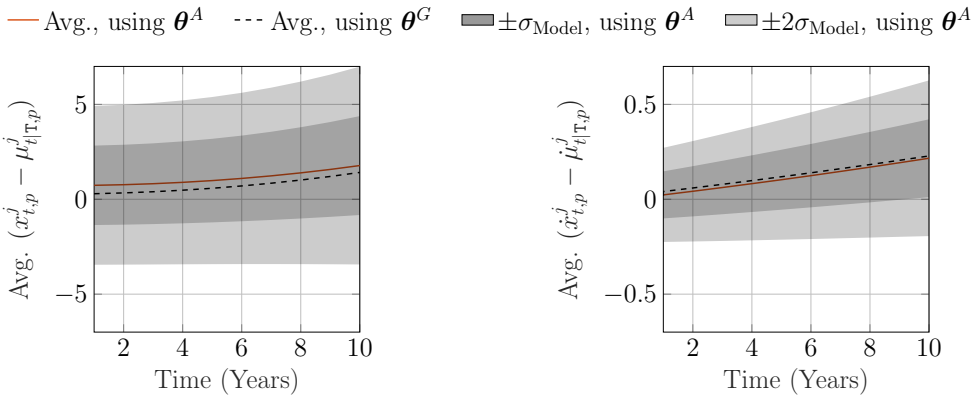

Figure 7: Average error in forecast for the degradation condition on the left and speed on the right, respectively, over 10 years, for the analytical framework in red, and gradient-based framework in black, with the confidence interval for the estimation $\pm 2\sigma$.

Table 1: Performance comparison for the different frameworks in the log-likelihood associated with the validation and test set.

Model	Log-likelihood	
	Test set	Validation set
Biased inspectors, $\mu_V(I_i) \neq 0$	-35850	-67916
Unbiased inspectors, $\mu_V(I_i) = 0$	-37100	-68410

biases from all inspectors is 0.12, and is represented by the dashed line. The maximum value of the absolute bias is $\max(|\mu_V(I_i)|) = 3.47$, while the majority of the estimated bias values are between -1 and $+1$. By comparing Figure 8b with 8c, it can be noticed that neglecting the bias enlarges the standard deviation estimates; this is due to the additional variability in the inspection data from inspectors having large bias values. In order to validate the estimation capacity of the gradient-based framework, the estimated parameters $\boldsymbol{\theta}^G$ are utilized to model the degradation of structural elements from the real database. An example for time series analyses using the estimated model parameters $\boldsymbol{\theta}^G$ and $\boldsymbol{\theta}^{G-}$ is shown in Figure 9, where the inspection data of element e_{128}^{56} in bridge b_{56} are employed to perform the degradation analysis using the SSM-KR framework, and the estimated parameters $\boldsymbol{\theta}^G$ and $\boldsymbol{\theta}^{G-}$. In Figure 9, in order to distinguish the bias estimated for each inspector, the observations corrected with inspectors' biases are represented by an asterisk. Moreover, the last inspection performed on this element in 2019 (represented by a red circle), was removed from the training set and was never used in the estimation of the model parameters nor in the degradation model in order to test the predictive capacity of the SSM-based model. By comparing the analysis considering biased inspectors (red circle markers) with the one relying on unbiased inspectors (black square markers), it can be noted that the addition of the bias improves the consistency with the hidden observation. Moreover, when the hidden observation is corrected with the inspector's bias, the degradation condition prediction overlaps with the hidden observation. The network-scale performance of the degradation model when considering biased inspectors and unbiased inspectors are reported in Table 1, where the log-likelihood associated with the validation and test set are shown. In both cases, the framework showing the best (i.e., the highest) log-likelihood is the one considering biased inspectors.

4.2.2 Real Inspector's Uncertainty Quantification Using the Analytical Framework

The analytical framework is validated first, by comparing the parameters $\boldsymbol{\theta}^A$ estimated using the analytical framework with $\boldsymbol{\theta}^G$ from the gradient-based framework, then, by evaluating the performance of the SSM-based model at predicting the degradation based on the estimated inspectors' uncertainty from $\boldsymbol{\theta}^A$ and $\boldsymbol{\theta}^G$. The inspectors' variables estimated

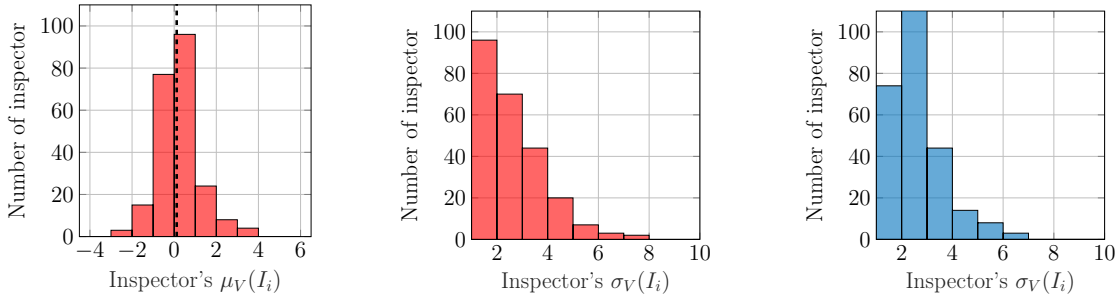

(a) Estimated biases

(b) Estimated standard deviations

(c) Estimated standard deviation while $\mu_V = 0$

Figure 8: Histograms for the estimation of the inspectors' parameters in the transformed space for the gradient-based framework. Figure (a) and (b) show the histogram for the estimated biases $\mu_V(I_i)$ and standard deviations $\sigma_V(I_i)$ respectively while considering biased inspectors, while Figure (c) shows the histogram for the estimated standard deviations $\sigma_V(I_i)$, when the inspectors are considered unbiased.

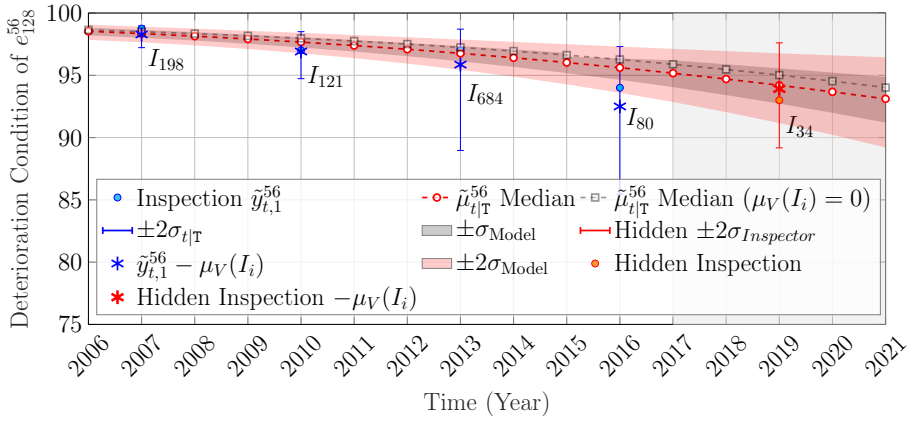

Figure 9: Deterioration state analysis for the condition of the structural element e_1^3 based on the inspections $\tilde{\boldsymbol{y}}_{t,1}^{53} \in [25, 100]$. The inspections $\tilde{\boldsymbol{y}}_{t,1}^{53}$ are represented by blue points, where the asterisks represent the correction associated with the estimated bias $\mu_V(I_i)$, and the error bars represent the inspectors' standard deviation. The red point shows the hidden inspection data that was removed from the training data in order to test the predictive capacity of the SSM-based model. The expected value for the model estimates for the condition $\tilde{\mu}_{t|\mathrm{T}}^{56}$ is shown in red dashed line when $\mu_V(I_i) \neq 0$, and in black when $\mu_V(I_i) = 0$. The red areas represent the confidence interval for σ_{Model} and $2\sigma_{\mathrm{Model}}$ while $\mu_V(I_i) \neq 0$.

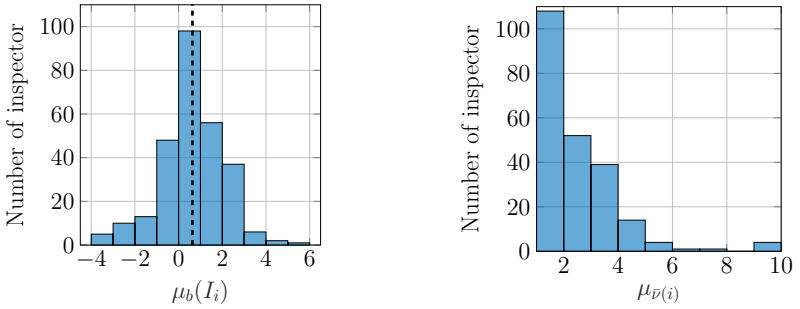

(a) Estimated biases

(b) Estimated standard deviations

Figure 10: Histograms for the estimation of the inspectors' variables $\boldsymbol{\theta}^A$ in the transformed space for the analytical framework while considering the relative biases. Figure (a) show the histogram for the estimated biases $\mu_V(I_i)$ and Figure (b), the estimated standard deviations $\sigma_V(I_i)$ respectively.

Table 2: Comparison for the computational time required for estimating the sets of inspectors' uncertainty $\boldsymbol{\theta}^v$ and model parameters $\boldsymbol{\theta}$ while using the analytical and gradient-based frameworks for estimating $\boldsymbol{\theta}^v$. The computational times are estimated using a system equipped with CPU Intel¬Æ$Xeon$¬Æ$CPUE5-2687Wv4, 256GBmemoryandNVIDIATeslaP40GPU$.

Method used for estimating $\boldsymbol{\theta}^v$	Time required for estimating Inspectors' parameters $\boldsymbol{\theta}^v$	All parameters $\boldsymbol{\theta}$
Gradient-based framework	33 hours	75 hours
Analytical framework	0.3 hours	43 hours

by the analytical framework are reported in Figure 10.
The average of the estimated biases is equal to 0.63 as represented by the dashed line in Figure 10, while the maximum bias value is $\max(|\mu_b(I_i)|) = 5.31$, and most of the estimated bias values are between -1 and 2.

By comparing the results obtained with the gradient-based framework in Figure 8, it can be noted that the histogram for the estimated biases is not exactly centered at zero; however, this shift is acceptable considering the range of the estimated bias values. The computational time for both frameworks is reported in Table 2. The time associated with the inspectors' variables corresponds to the time required for estimating the inspectors' parameters for all epochs, while the total time is for the estimation of the entire set of model parameters $\boldsymbol{\theta}$, which includes the SSM parameters $\boldsymbol{\theta}^s$, the inspectors' variables $\boldsymbol{\theta}^A$ or $\boldsymbol{\theta}^G$, and the vector of kernel regression parameters $\boldsymbol{\theta}^k$. Replacing the gradient-based framework by the analytical framework in the SSM-based model reduces the total computational

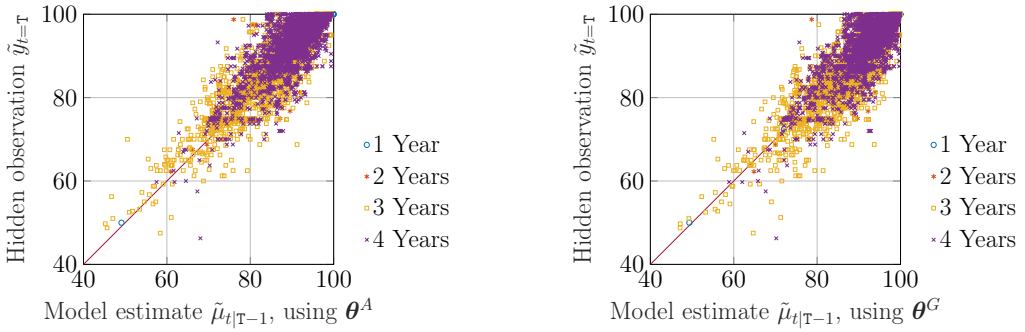

(a) Analytical framework

(b) Gradient-based framework

Figure 11: Forecast estimation of the degradation condition versus hidden observation with different forecast period of the SSM-based model using the estimated parameters of the analytical framework $\boldsymbol{\theta}^A$ in Figure (a), and gradient-based frameworks $\boldsymbol{\theta}^G$ in Figure (b).

time by 42%. In the gradient-based framework, the estimation of the inspectors' variables represents 44% of the computational time where for the analytical frameworks it is less than 1%.

In order to assess the predictive capacity of the SSM-based method using the variables $\boldsymbol{\theta}^A$, the last inspection $\tilde{y}_{\mathtt{T}}$ of the elements where removed from the training set of the degradation model. Figure 11a shows a scatter plot comparing the condition states $\tilde{\mu}_{t|\mathtt{T}-1}$ estimated from the data available until $\mathtt{T}-1$ with the corresponding hidden observations $\tilde{y}_{\mathtt{T}}$. Figures 11b shows the same scatter plot for the SSM-based model using the parameters $\boldsymbol{\theta}^G$. The forecast period can differs for each structural element, as the number of years between two consecutive inspections is not the same for every bridges. Each type of marker corresponds to the number of years for the forecast period, (i.e., the number of years between the last observation used in the training and the hidden observation).

From Figure 11a, the predictive capacity of the SSM-based model shows no difference with respect to the forecast time. It should be noted that the predictions are not required to match the inspection data given that the observations do not represent the true state of the element, which is unobservable in practice. Moreover, by comparing Figure 11a with Figure 11b, the model predictive capacity is not altered by the use of the analytical framework instead of the gradient-based one for estimating the inspectors' uncertainty.

The network-scale performance of the analytical framework is evaluated by the log-likelihood for the test set associated with the SSM-KR model while using $\boldsymbol{\theta}^G$ or $\boldsymbol{\theta}^A$, which are reported in Table 3. Even though the gradient-based framework shows a better log-likelihood for the test set compared with the analytical framework, the analytical framework's predictive capacity is still acceptable considering the results from Figure 11, and the improvements in the computational time shown in Table 2.

Table 3: Performance comparison for the SSM-based framework in the log-likelihood associated with the test set, while using the estimates from the analytical and gradient-based frameworks.

Parameters used in the SSM-based model	Log-likelihood for the test set
$\boldsymbol{\theta}^G$	-35850
$\boldsymbol{\theta}^A$	-36220

5 Conclusion

This paper has examined the inspectors' uncertainty in the context of visual inspections on transportation infrastructure. To that end, two frameworks were developed for estimating the inspectors' relative biases and standard deviations. The first framework relies on the MLE approach that is already employed for estimating the SSM-based model parameters, while the second framework is based on the AGVI estimation framework as well as the Kalman update step. The verification and validation analyses performed on synthetic and real databases have led to the conclusion that the inclusion of the inspectors' relative bias in the degradation model improves the overall predictive capacity of the framework. These improvements are demonstrated by an overall reduction in errors for the synthetic case, and an increased log-likelihood for the test set for the real data. Moreover, both the analytical and gradient-based frameworks proved to be effective in quantifying the inspectors' relative biases. The analytical framework implementation provides a significant gain in the computational time required for the inspectors' uncertainty estimation (i.e., reducing from 33 hours to 20 minutes), however, the accuracy of the parameters estimation is slightly reduced in comparison with the gradient-based framework. The total computational time is reduced by 40% for the real data when using the analytical framework for estimating the inspectors' uncertainty. The main limitations of the propose analytical framework are related to the initialization of the hidden states associated with the biases and variances, as well as the assumption that globally, the inspectors are unbiased and only their relative bias are estimated. Overall, we recommend using the analytical approach for estimating the inspectors' uncertainty. Even though the predictive capacity of the SSM-KR using the parameters estimated by the gradient-based framework have shown a better consistency, the analytical framework estimations remains satisfactory and the gain in the computational cost compensates for the reduced accuracy.

Acknowledgements

This project is funded by the Transportation Ministry of Quebec Province (MTQ), Canada. The authors would like to acknowledge the support of Simon Pedneault for facilitating the

access to the inspections database employed in this paper.

References

[1] Bryan T Adey and Rade Hajdin. Methodology for determination of financial needs of gradually deteriorating bridges with only structure level data. *Structure and Infrastructure Engineering*, 7(7-8):645–660

[2] Duzgun Agdas, Jennifer A Rice, Justin R Martinez, and Ivan R Lasa. Comparison of visual inspection and structural-health monitoring as bridge condition assessment methods. *Journal of Performance of Constructed Facilities*, 30(3):04015049, 2015.

[3] Farhad Ansari. *Sensing issues in civil structural health monitoring*, volume 1. Springer, 2005.

[4] Erica Arango, Mónica Santamaria, Hélder S Sousa, and José C Matos. *Reliability-Based Bayesian Updating Using Visual Inspections of Existing Bridges*. Springer, 2021.

[5] James MW Brownjohn. Structural health monitoring of civil infrastructure. *Philosophical Transactions of the Royal Society A: Mathematical, Physical and Engineering Sciences*, 365(1851):589–622, 2007.

[6] Wei Chen and Shuping Huang. Human reliability analysis for visual inspection in aviation maintenance by a Bayesian network approach. *Transportation Research Record*, 2449(1):105–113, 2014.

[7] Bhargob Deka. *Analytical Bayesian Parameter Inference for Probabilistic Models with Engineering Applications*. PhD thesis, Polytechnique Montréal, Montréal, Canada, 2022.

[8] Michael P Enright and Dan M Frangopol. Condition prediction of deteriorating concrete bridges using Bayesian updating. *Journal of Structural Engineering*, 125(10): 1118–1125, 1999.

[9] Charles R Farrar and Keith Worden. *Structural health monitoring: a machine learning perspective*. John Wiley and Sons, 2012.

[10] Matthew S. Gralund and Jay A. Puckett. System for bridge management in a rural environment. *Journal of Computing in Civil Engineering*, 10(2):97–105, 1996.

[11] Benjamin A Graybeal, Brent M Phares, Dennis D Rolander, Mark Moore, and Glenn Washer. Visual inspection of highway bridges. *Journal of Nondestructive Evaluation*, 21(3):67–83

[12] Zachary Hamida and James-A Goulet. Modeling infrastructure degradation from visual inspections using network-scale state-space models. *Structural Control and Health Monitoring*, pages 1545–2255, 2020.

[13] Zachary Hamida and James-A Goulet. Network-scale deterioration modelling based on visual inspections and structural attributes. *Structural Safety*, 2020.

[14] Zachary Hamida and James-A. Goulet. Quantifying the effects of interventions based on visual inspections of bridges network. *Structure and Infrastructure Engineering*, pages 1–12, 2021.

[15] Philipp Hüthwohl, Ioannis Brilakis, André Borrmann, and Rafael Sacks. Integrating RC bridge defect information into BIM models. *Journal of Computing in Civil Engineering*, 32(2):04018013, 2018.

[16] Robert I Jennrich and Stephen M Robinson. A Newton-Raphson algorithm for maximum likelihood factor analysis. *Psychometrika*, 34(1):111–123 1860–0980, 1969.

[17] JD Kalbfleisch and Jerald F Lawless. The analysis of panel data under a Markov assumption. *Journal of the American Statistical Association*, 80(392):863–871

[18] Rudolf Emil Kalman. Contributions to the theory of optimal control. *Bol. Soc. Mat. Mexicana*, 5(2):102–119, 1960.

[19] H Korving and JM Van Noortwijk. Bayesian updating of a prediction model for sewer degradation. *Urban Water Journal*, 5(1):51–57, 2008.

[20] Hong-Nan Li, Liang Ren, Zi-Guang Jia, Ting-Hua Yi, and Dong-Sheng Li. State-of-the-art in structural health monitoring of large and complex civil infrastructures. *Journal of Civil Structural Health Monitoring*, 6(1):2190–5479, 2016.

[21] Min Li and Gaofeng Jia. Bayesian Updating of Bridge Condition Deterioration Models using Complete and Incomplete Inspection Data. *Journal of Bridge Engineering*, 25 (3):1084–0702, 2020.

[22] Mehdi Mohammadpour Lima, Dane Miller, and Jeung-Hwan Doh. Structural health monitoring of concrete bridges in guilan province based on a visual inspection method. *Structural Durability and Health Monitoring*, 9(4):269

[23] Mark Moore, Brent M Phares, Benjamin Graybeal, Dennis Rolander, Glenn Washer, Janney Wiss, et al. Reliability of visual inspection for highway bridges, volume i. Technical report, Turner-Fairbank Highway Research Center, 2001.

[24] MTQ. *Manuel d'Inspection des Structures*. Ministère des Transports, de la Mobilité Durable et de l'Électrification des Transports, Jan 2014.

[25] Brent M. Phares, Glenn A. Washer, Dennis D. Rolander, Benjamin A. Graybeal, and Mark Moore. Routine highway bridge inspection condition documentation accuracy and reliability. *Journal of Bridge Engineering*, 9(4):403–413, 2004.

[26] Herbert E Rauch, CT Striebel, and F Tung. Maximum likelihood estimates of linear dynamic systems. *AIAA journal*, 3(8):1445–1450 0001–1452, 1965.

[27] Dan Simon and Donald L Simon. Constrained Kalman filtering via density function truncation for turbofan engine health estimation. *International Journal of Systems Science*, 41(2):159–171

[28] Jian Wang and Xila Liu. Evaluation and Bayesian dynamic prediction of deterioration of structural performance. *Structure and Infrastructure Engineering*, 6(6):663–674, 2010.

[29] Shuyuan Xu, Jun Wang, Xiangyu Wang, Peng Wu, Wenchi Shou, and Chao Liu. A parameter-driven method for modeling bridge defects through IFC. *Journal of Computing in Civil Engineering*, 36(4):04022015, 2022.

[30] Mariano Angelo Zanini, Flora Faleschini, and Carlo Pellegrino. Bridge residual service-life prediction through Bayesian visual inspection and data updating. *Structure and Infrastructure Engineering*, 13(7):906–917, 2017.

A Kalman Filter and Kalman Smoother Equations

The Kalman filter (KF) enables estimating the hidden state $\boldsymbol{x}_t$ at time t using two steps, the prediction step and the update step. The prediction step describes the transition from $\boldsymbol{x}_{t-1}$ using a transition matrix $\boldsymbol{A}^{\mathtt{ki}}$ as in,

$$\begin{aligned} \mathbb{E}[\boldsymbol{X}_t|\boldsymbol{y}_{1:t-1}] &\equiv \boldsymbol{\mu}_{t|t-1} = \boldsymbol{A}^{\mathtt{ki}}\boldsymbol{\mu}_{t-1|t-1} \\ \mathrm{cov}[\boldsymbol{X}_t|\boldsymbol{y}_{1:t-1}] &\equiv \boldsymbol{\Sigma}_{t|t-1} = \boldsymbol{A}^{\mathtt{ki}}\boldsymbol{\Sigma}_{t-1|t-1}\boldsymbol{A}^{\mathtt{ki},\intercal} + \boldsymbol{Q}^{\mathtt{ki}}, \end{aligned} \tag{15}$$

where $\mathbb{E}[\boldsymbol{X}_t|\boldsymbol{y}_{1:t-1}]$ is the expected value the hidden state vector $\boldsymbol{x}_t$ at time t given all the observations $\boldsymbol{y}_{1:t-1}$ up to time $t-1$, $\mathrm{cov}[\boldsymbol{X}_t|\boldsymbol{y}_{1:t-1}]$ is covariance of the hidden state vector $\boldsymbol{x}_t$, and $\boldsymbol{Q}^{\mathtt{ki}}$ is the covariance matrix of the process error. The transition matrix $\boldsymbol{A}^{\mathtt{ki}}$ is described by,

$$\boldsymbol{A}^{\mathtt{ki}} = \begin{bmatrix} 1 & \Delta t & \frac{\Delta t^2}{2} \\ 0 & 1 & \Delta t \\ 0 & 0 & 1 \end{bmatrix}, \tag{16}$$

where dt is the time step, and $\boldsymbol{I}$ is the identity matrix and. On the other hand, the covariance matrix $\boldsymbol{Q}^{\mathtt{ki}}$ is defined as in,

$$\boldsymbol{Q}^{\mathtt{ki}} = \sigma_w^2 \begin{bmatrix} \frac{\Delta t^4}{4} & \frac{\Delta t^3}{2} & \frac{\Delta t^2}{2} \\ \frac{\Delta t^3}{2} & \Delta t^2 & \Delta t \\ \frac{\Delta t^2}{2} & \Delta t & 1 \end{bmatrix}, \tag{17}$$

where σ_w is a model parameter that describe the standard deviation of the kinematic model process error and $\boldsymbol{Q}^r$ is a diagonal matrix of model parameters describing the intervention errors at the element-level [14]. After the prediction step, updating the model estimate with observations at time t is possible by using the update step,

$$\begin{aligned} f(\boldsymbol{x}_t|\boldsymbol{y}_{1:t}) &= \mathcal{N}(\boldsymbol{x}_t; \boldsymbol{\mu}_{t|t}, \boldsymbol{\Sigma}_{t|t}) \\ \boldsymbol{\mu}_{t|t} &= \boldsymbol{\mu}_{t|t-1} + \boldsymbol{K}_t(\boldsymbol{y}_t - \boldsymbol{C}\boldsymbol{\mu}_{t|t-1}) \\ \boldsymbol{\Sigma}_{t|t} &= (\boldsymbol{I} - \boldsymbol{K}_t\boldsymbol{C})\boldsymbol{\Sigma}_{t-1|t-1} \\ \boldsymbol{K}_t &= \boldsymbol{\Sigma}_{t-1|t-1}\boldsymbol{C}^\intercal\boldsymbol{G}_t^{-1} \\ \boldsymbol{G}_t &= \boldsymbol{C}\boldsymbol{\Sigma}_{t-1|t-1}\boldsymbol{C}^\intercal + \boldsymbol{R}_t, \end{aligned} \tag{18}$$

where the posterior estimates $\boldsymbol{\mu}_{t|t} \equiv \mathbb{E}[\boldsymbol{X}_t|\boldsymbol{y}_{1:t}]$ and $\boldsymbol{\Sigma}_{t|t} \equiv \mathrm{cov}[\boldsymbol{X}_t|\boldsymbol{y}_{1:t}]$ are represented by the expected value and covariance at time t, conditional to the observations up to time t, the Kalman gain is represented by $\boldsymbol{K}_t$, and $\boldsymbol{G}_t$ is the innovation covariance. Following the filtering step, the RTS Kalman smoother (KS) [26] is applied as a backward framework which relies on the information from all the observations up to time $t = \mathtt{T}$, to update the

previous hidden states estimates. The equations of the KS are described as in,

$$\begin{aligned} f(\boldsymbol{x}_t|\boldsymbol{y}_{1:\mathtt{T}}) &= \mathcal{N}(\boldsymbol{x}_t; \boldsymbol{\mu}_{t|T}, \boldsymbol{\Sigma}_{t|T}) \\ \boldsymbol{\mu}_{t|\mathtt{T}} &= \boldsymbol{\mu}_{t|t} + \boldsymbol{J}_t(\boldsymbol{\mu}_{t+1|\mathtt{T}} - \boldsymbol{\mu}_{t+1|t}) \\ \boldsymbol{\Sigma}_{t|\mathtt{T}} &= \boldsymbol{\Sigma}_{t|t} + \boldsymbol{J}_t(\boldsymbol{\Sigma}_{t+1|\mathtt{T}} - \boldsymbol{\Sigma}_{t+1|t})\boldsymbol{J}_t^{\mathsf{T}} \\ \boldsymbol{J}_t &= \boldsymbol{\Sigma}_{t|t}\boldsymbol{A}^{\mathtt{ki},\mathsf{T}}\boldsymbol{\Sigma}_{t+1|t}^{-1}. \end{aligned} \tag{19}$$

B Transformation Function

The transformation function $o(\tilde{x})$ maps a deterioration state from the bounded space $\tilde{x} \in [l, u]$ to the unbounded space $x \in [-\infty, \infty]$, while the function $o^{-1}(x)$ enables reversing the aforementioned operation. The functions $o(\tilde{x})$ and $o^{-1}(x)$ are described according to Hamida:2020aa by the equations,

$$x = o(\tilde{x}) = \begin{cases} \left[\frac{1}{\Gamma(\alpha)}\int_0^{\tilde{x}} t^{\alpha-1}e^{-t}dt\right]^{\alpha}, & \frac{u+l}{2} < \tilde{x} \leq u, \\ \tilde{x}, & \tilde{x} = \frac{u+l}{2}, \\ -\left[\frac{1}{\Gamma(\alpha)}\int_0^{\tilde{x}} t^{\alpha-1}e^{-t}dt\right]^{\alpha}, & l \leq \tilde{x} < \frac{u+l}{2}, \end{cases} \qquad \tilde{x} = o^{-1}(x) = \begin{cases} \frac{1}{\Gamma(\alpha)}\int_0^{x^{\frac{1}{\alpha}}} t^{\alpha-1}e^{-t}dt, & x > \frac{u+l}{2}, \\ x, & x = \frac{u+l}{2}, \\ -\frac{1}{\Gamma(\alpha)}\int_0^{x^{\frac{1}{\alpha}}} t^{\alpha-1}e^{-t}dt, & x < \frac{u+l}{2}. \end{cases} \tag{20}$$

Note that α is given by: $\alpha = 2^{-n}$, where n is a model parameter defined as a positive integer in the range $n \in [1, 6]$.

C Full Analytical Framework for Estimating the Inspectors' Bias and Variance

Figure 12 illustrates the steps for the estimation process using the proposed analytical framework based on the inspection data from a single bridge $\mathcal{B}_j$. The flowchart on the left side shows the sequential updates for the variables $v(I_{1:\mathtt{I}})$ associated with each inspector. For an element $e_p^j \in \mathcal{B}_j$, if an inspection y_t is available at year t, the variable $v(I_i)$ associated with the inspector I_i is updated. The steps for updating $v(I_i)$ for a single inspector I_i at year t, are outlined in the flowchart on the right side of Figure 12. The first step corresponds to the update of the variables $v_{\bar{\nu}(i)}$ and $v_b(I_i)$ using the Kalman update step. Thereafter, the variable $v_{\bar{\nu}(i)}$ is updated with the additional AGVI update step. Following the aforementioned update steps, it is possible to obtain v_s from $v_{\bar{\nu}(i)}$, where $\sigma_s^2 = \mu_{\bar{\nu}(i)}$ and $\mu_s = 0$. The resulting estimate for the inspector's uncertainty $v(I_i)$ at time t is computed by the summation of v_b and v_s. These update steps are performed recursively over time for each element in the bridge $\mathcal{B}_j$. In order to apply the methodology over the entire set of bridges $\mathcal{Q}$, the same process is repeated sequentially for each bridge $\mathcal{B}_j \in \mathcal{Q}$.

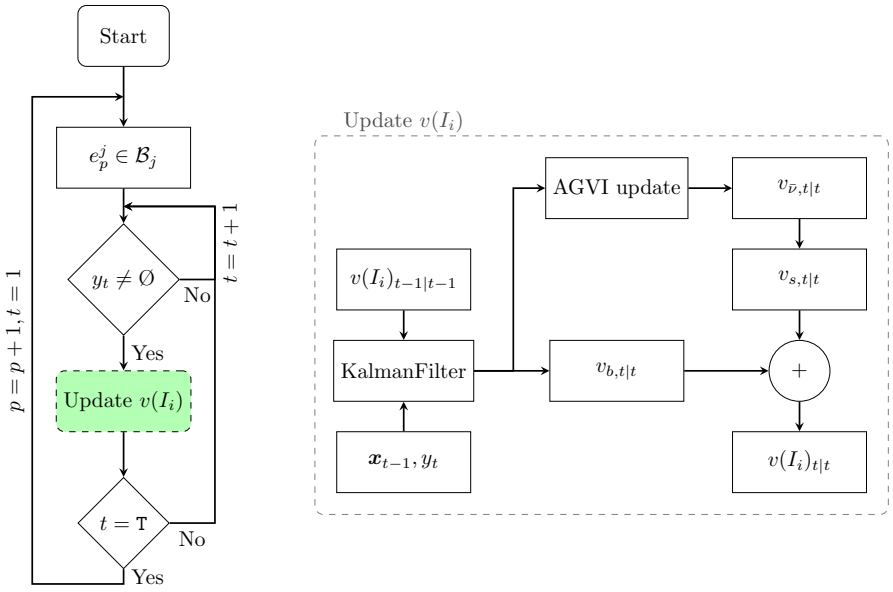

Figure 12: Flowchart for the estimation of the inspectors' uncertainty using the analytical framework and the inspection data of a single bridge $\mathcal{B}_j$. On the left, the flowchart presents the iterations performed within the bridge inspection data for estimating the entire set of inspectors' variables $v(I_{i:\mathtt{I}})$. On the right, the flowchart outlines the steps corresponding to the estimation of a single inspector's uncertainty $v(I_i)$ at a given time t.

D Incorporation of the Analytical Method within the Parameter Estimation Framework for the SSM-KR Model

The estimation of the set of parameter $\boldsymbol{\theta} = \{\boldsymbol{\theta}^s, \boldsymbol{\theta}^k, \boldsymbol{\theta}^v\}$ is done over multiple epochs, where $\boldsymbol{\theta}^s = \{\sigma_W, n, \sigma_0, \ddot{\sigma}_0, p_1, p_2, \sigma_V\}$ associated with the degradation model, $\boldsymbol{\theta}^k = \{\sigma_{w0}, \boldsymbol{\ell}\}$ associated with the kernel regression framework and $\boldsymbol{\theta}^v = \{\mu_V(I_{i:\mathtt{I}}), \sigma_V(I_{i:\mathtt{I}})\}$ associated with the inspectors uncertainty are estimated successively, while the other sets remain fixed.

Algorithm 1 Incorporation of the Analytical Method within the estimation framework for the SSM-KR model

Require: $\boldsymbol{\theta}^s_0$: Initial SSM parameters
Require: $\boldsymbol{\theta}^k_0, \dot{\boldsymbol{x}}_{\boldsymbol{z}}$: Initial KR parameters and state respectively
Require: $\boldsymbol{x}_0, \ddot{\boldsymbol{x}}_0$: Initial state for condition and acceleration

$\boldsymbol{\theta}^s_1 \leftarrow \text{NewtonRaphson}(\mathcal{L}(\boldsymbol{\theta}^s), \boldsymbol{\theta}^s_0, \nu_1)$
$\mu_{V_s}(I_{1:\mathtt{I}}) = \sigma_V,\ \sigma_V \in \boldsymbol{\theta}^s_1,\ \sigma_{V_b}(I_{1:\mathtt{I}}) = 12$
$\mu_{V_b}(I_{1:\mathtt{I}}) = 0,\ \sigma_{V_b}(I_{1:\mathtt{I}}) = 1$
$L_1 \leftarrow -10^{12}$ (Initial *log-likelihood*), $L_2 \leftarrow \mathcal{L}(\boldsymbol{\theta}^s_1)$, $\epsilon \leftarrow 0.999$ (Convergence tolerance)
$j \leftarrow 1$
while $(L_{j+1}/L_j) \leq \epsilon$ **do**
    while $(L_{j+1}/L_j) \leq \epsilon$ **do**
        $L_j \leftarrow L_{j+1}$
        for $p := 1$ to $\mathtt{E}$ **do**
            for $t := 1$ to $\mathtt{T}$ **do**
                if $j = 1$ **then**
                $\mu_V(I_i), \sigma_V(I_i), \boldsymbol{x}_{t+1,p} \leftarrow \text{AnalyticalFramework}(y_{t,p}, \boldsymbol{x}_{t,p}, \boldsymbol{\theta}^s_j)$
                else
                $\mu_V(I_i), \sigma_V(I_i), \boldsymbol{x}_{t+1,p} \leftarrow \text{AnalyticalFramework}(y_{t,p}, \boldsymbol{x}_{t,p}, \boldsymbol{\theta}^s_j, \boldsymbol{\theta}^k_j, \dot{\boldsymbol{x}}_{\boldsymbol{z}})$
        $L_{j+1} \leftarrow \mathcal{L}(\mu_V(I_i), \sigma_V(I_{1:\mathtt{I}}))$
    if $j = 1$ **then**
        $\boldsymbol{\theta}^s_{j+1} \leftarrow \text{NewtonRaphson}(\mathcal{L}(\boldsymbol{\theta}^s_j), \boldsymbol{\theta}_j, \nu_1)$
    else $\boldsymbol{\theta}^s_{j+1} \leftarrow \text{NewtonRaphson}(\mathcal{L}(\boldsymbol{\theta}^s_j, \dot{\boldsymbol{x}}_{\boldsymbol{z}}), \boldsymbol{\theta}_j, \nu_1)$
    $[\boldsymbol{\theta}^k_{j+1}, \dot{\boldsymbol{x}}_{\boldsymbol{z}}] \leftarrow \text{NewtonRaphson}(\mathcal{L}(\boldsymbol{\theta}^k_j, \text{RecursiveEstimation}(\dot{\boldsymbol{x}}_{\boldsymbol{z}})), \boldsymbol{\theta}_j, \nu_1)$
    $L_j \leftarrow \mathcal{L}(\boldsymbol{\theta}_{j+1})$
    $j \leftarrow j + 1$
return $\boldsymbol{\theta}_{j+1}$ and $\dot{\boldsymbol{x}}_{\boldsymbol{z}}$ (Resulting parameters)